Crossover from Reverse Saturable to Saturable Absorptions in Two-Dimensional Tungsten Disulfide

T. Neupane and C. M. Adhikari

Journal of Nepal Physical Society
Volume 8, No 2, 2022
(Special Issue: ANPA Conference 2022)
ISSN: 2392-473X (Print), 2738-9537 (Online)

JNPS, **8** (2), 31-36 (2022)
DOI: http://doi.org/10.3126/jnphyssoc.v8i2.50145

Published by: Nepal Physical Society
P.O. Box: 2934
Tri-Chandra Campus
Kathmandu, Nepal
Email: nps.editor@gmail.com

ANPA Conference 2022
ISSN : 2392-473X(Print), 2738-9537 (Online)

Research Article ©Nepal Physical Society
DOI:http://doi.org/10.3126/jnphyssoc.v8i2.50145

Crossover from Reverse Saturable to Saturable Absorptions in Two-Dimensional Tungsten Disulfide

T. Neupane[1, a)] and C. M. Adhikari[2]

[1)] *Chemistry and Physics Department, The University of North Carolina at Pembroke, Pembroke, NC 28372, USA*
[2)] *Department of Chemistry, Physics and Materials Science, Fayetteville State University, Fayetteville, NC 28301, USA*

[a)] *Corresponding author: tikaram.neupane@uncp.edu*

Abstract. The Tungsten disulfide atomic layer has enormous scientific merits that play a key role in the nonlinear absorption process. Four distinct excitonic peaks in the absorption spectra are crucial for identifying the polarity of nonlinear absorption by virtue of the resonant or non-resonant excitation process. The excitation source of 532 nm is enough for the one-photon optical transition at both low-energy excitonic peaks and two-photon transition at both higher-energy excitonic peaks. The Tungsten disulfide atomic layer exhibited the reverse saturable (or positive nonlinear) absorption through the two-step excitation process which could be possible due to the optical transition at the higher energy excitonic peaks. In addition, the polarity of the nonlinear absorption coefficient and its interchange have been analytically studied with the aid of a magnitude of excited-state absorption cross-section and Ground-state absorption cross-section. Besides, the various possible factors affecting the Z-scan results are discussed.

Received: 30 August 2022; **Accepted**: 14 October 2022; **Published**: 31 December 2022

Keywords: Atomic layer; Excitonic peaks; One-photon and two-photon excitation process.

INTRODUCTION

The nonlinear absorption (NLA) properties of the tungsten disulfide (WS_2) atomic layer have emerged as an important research topic because of their optoelectronic and photonic applications [1-5]. Recently, the third-order nonlinear optical properties, which include the polarity and magnitude of NLA and nonlinear refraction (NLR) of the optical medium, have been explored extensively for both cases of inversion symmetry and asymmetry in the WS_2 atomic layers [2, 6]. The polarity of NLA is a prime factor for prospective technical application in optoelectronics. For example, the saturable absorption (SA) of negative nonlinearity materials are used for the lasers as Q-switching elements [7] and the reverse saturable absorption (RSA) of positive nonlinearity materials are applicable for two-photon microscopy and optical limiters [8]. Therefore, the "Z-scan technique" is used to investigate the polarity of NLA coefficient which is comparatively simple and more accurate compared to other third-order nonlinear characterization techniques [9, 10]. The WS_2 atomic layers have scientific merits due to the layer dependent direct/indirect band gap and their corresponding optical transition [11]. In addition, the optical spectra of WS_2 atomic layer show mainly four distinct absorption peaks "A", "B", "C", and "D" appearing at 627, 520, 457, and 345 nm respectively as shown in Fig. 1 [5]. The layer-dependent optical transition in WS_2 atomic layer with specified four excitonic peaks decides the polarity of NLA through a resonant and non-resonant transition process for a given excitation energy. Therefore, the excitation source is one of the key factors affecting magnitude and polarity of NLA. The literature review revealed that the saturable absorption characteristics is prevailed via the one-photon absorption (OAP) process [1, 12]. At the same time, the RSA is observed through the two-photon absorption and/or two-step excitation due to the larger absorption cross-section in the excited state than that of the ground state [12, 13]. In the one-photon excitation process, the electric dipole transition from initial to the final state is possible due to the different parities between them. Therefore the ground-state absorption (GSA) cross-section is higher than the excited-state absorption (ESA) cross-section resulting in the dominant SA characteristics. However, in the two-photon excitation process, the electric dipole transitions

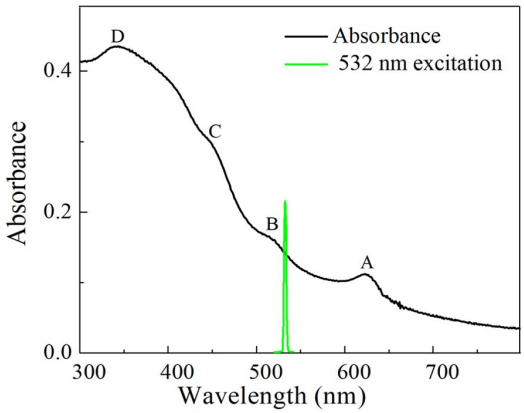

FIGURE 1. Linear absorption spectrum of the WS_2 Atomic layer (black) and excitation source (green). The absorption spectrum is adapted from the published paper to put on view of "A", "B", "C", and "D" excitonic peaks [5].

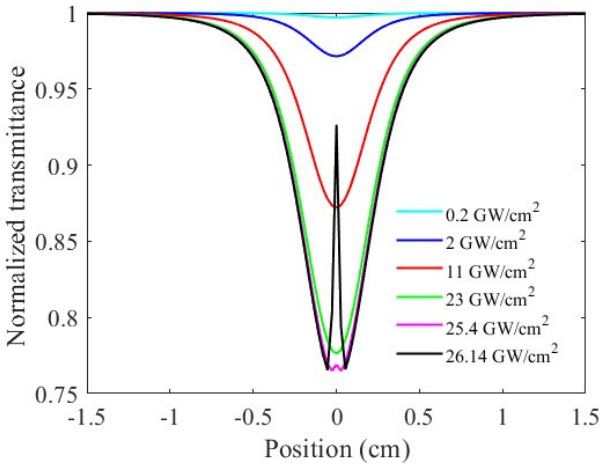

FIGURE 2. Nonlinear transmittance as a function of sample position for given excitation intensities.

from the initial to the final state are allowed due to the same parities between them via the different parity of an intermediate state. It implies that the excited state absorption cross-section is higher than that of the ground state, which consequences the RSA. Therefore, the excitation source at 532 nm is considered a resonant excitation source for the OPA process if only A and B excitonic peaks are considered. However, the situation might be different if C and D excitonic peaks are included in the optical transition process. It intimates that the requirements of excitation energy, in the WS_2 atomic layer, for the resonant and non-resonant excitation process could be rescaled if excitonic peaks at C and D are included. Neupane et al hypothesized the inclusion of excitonic peaks at C and D in the nonlinear optical transition for the first time, and then this work analytically extended the effect of the GSA and ESA on the crossover from RSA to SA and vice versa [5].

ANALYTICAL METHOD

The nonlinear absorption of the WS_2 atomic layer was analyzed by the open Z-scan technique for visible excitation source. It was a pulsed laser at 532 nm, 10 Hz repetition rate, and 6 ns temporal pulse width generated by Continuum surelite^{TM} II-10 laser system with the beam divergence < 0.5 mrad. The open Z-scan technique characterizes the polarity and magnitude of NLA. It measures the normalized transmittance as a function of sample position moving across the focusing point of laser axis (or z-axis) using a Gaussian beam. The Gaussian beam was prepared using two-irises method [5]. The beam profiles and images were captured by a CMOS Beam Profiling Camera (USB 3.0, Edmunds). The diameter of the Gaussian beam at the focusing lens plane was 2.6 mm at FWHM of the Gaussian profile. The radius of a beam at the focal point (w_0) is estimated by, $w_0^2 = \frac{f/z_1}{\sqrt{1+\left(\frac{f}{z_1}\right)^2}} r^2$, where $z_1 = \frac{\pi r^2}{\lambda}$, r is a radius of a beam at focusing lens plane, λ is the wavelength of a beam, and $f =$ 125 mm is the effective focal length of focusing lens. The radius of beam waist at the focal point was estimated to be 15.1 μm.

The normalized nonlinear transmittance (T) with open Z-scan is given by [9],

$$T(z,S=1) = \sum_{m=0}^{\infty} \frac{\left(\frac{-q}{1+(z/z_0)^2}\right)^m}{(1+m)^{3/2}}, \qquad (1)$$

for all $q < 1$ where $q(r,z,t) = \beta I_0 L_{\text{eff}}$ with, I_0 being the peak excitation intensity of input laser beam, β is the nonlinear absorption coefficient, and L_{eff} being longitudinal displacement of the sample from focus point given by $L_{\text{eff}} = \frac{1-exp(-\alpha_0 L)}{\alpha_0 L}$. Here, L is the sample thickness and α_0 is the linear absorption coefficient. To keep the beam size constant throughout the sample, the condition for the thin sample approximation should be valid i.e., the sample thickness is much less than Rayleigh's range $z_0 = \frac{kw_0^2}{2}$, where k is the wave number.

The intensity dependent total absorption coefficient $\alpha(I)$ can be written in terms of incident intensity I, saturation intensity I_s, and nonlinear absorption coefficient β as [14]

$$\alpha(I) = \frac{\alpha_0}{1+I/I_s} + \beta I, \qquad (2)$$

such that one can evaluate β as

$$\begin{aligned}\beta &= \frac{1}{I}\left(\alpha(I) - \frac{\alpha_0}{1+I/I_s}\right) \\ &= \frac{1}{I}\left(\sigma_{\rm esa}N_{ex} - \sigma_{\rm gsa}N_0 - \frac{\sigma_{\rm gsa}N_0}{1+I/I_s}\right), \end{aligned} \quad (3)$$

where $\sigma_{\rm gsa}$ and $\sigma_{\rm esa}$ are GSA and ESA cross sections respectively, and N_0 and N_{ex} are the carrier densities in the ground state and the excited state respectively. At a relatively lower excitation source, the carrier density at the excited state can be approximated by its ground state carrier density. Eq.(3) describes the contribution of absorption cross-section to distinguish the polarity of nonlinear absorption coefficient. We have used wavelength of 532 nm, laser pulse of width 6 ns, laser repetition rate of 10 Hz, beam radius of 1.12 mm at lens plane, 12.5 cm of the focal length of lens, sample length of 1 mm, and β of magnitude 6.0×10^{-8} m/W as fitting parameters as presented in Refs. [5, 15].

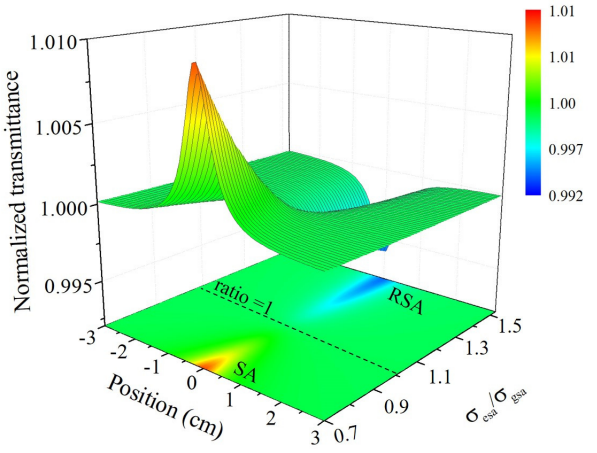

FIGURE 3. The nonlinear transmittance as the function of sample position and ratio of the ESA to GSA cross-section for 0.2 GW/cm^2 excitation intensity.

RESULT AND DISCUSSION

The WS_2 atomic layer includes 1 – 4 atomic layers with lateral size of 50 – 150 nm in the ethanol and water mixture, brought from the commercial product of Graphene supermarket, which was prepared by a liquid exfoliation [16]. The absorption spectrum of WS_2 atomic layer is shown in Fig.1. The absorption peaks at ∼627 and ∼520 nm are assigned to the optical transitions at K-position in momentum space due to the strong spin-orbit coupling [5, 11, 17, 18]. In specific, the A (∼627 nm) and B (∼520 nm) absorption peaks are allocated to the transition from the highest energy level in the valence band to the lowest conduction band and from the second highest energy level in the valence band to the lowest conduction band, respectively. The excitonic peaks at ∼457 and ∼345 nm attribute to the optical transitions due to the band nesting at the region where conduction and valence bands are parallel to each other in the momentum space [19, 20].

The normalized nonlinear transmittance for the various excitation intensities as a function of the sample position (z) is shown in Fig. 2. It exhibits the reverse saturable absorption or positive nonlinear absorption features for all given excitation intensities implying that the ESA cross section is higher than the GSA. As shown in Fig. 2, the magnitude of normalized nonlinear transmittance is decreased with an increase in the applied intensities. However, with the two highest intensities at 25.5 and 26.14 GW/cm^2, no further deeper valley traces are observed because of the existence of saturable absorption (SA) within an RSA [21] even in the two-step excitation process.

To the third order approximation, the transition rate Γ_{if} from an initial state $|i\rangle$ to the final state $|f\rangle$ is given by [22]

$$\begin{aligned}\Gamma_{if} &= \frac{2\pi}{\hbar}\left|\langle f|\,H'\,|i\rangle + \frac{1}{\hbar}\sum_n \frac{\langle f|\,H'\,|n\rangle\langle n|\,H'\,|i\rangle}{\omega_i-\omega_n}\right. \\ &+ \left.\frac{\rm i}{\hbar^2}\sum_n\sum_m \frac{\langle f|\,H'\,|m\rangle\langle m|\,H'\,|n\rangle\langle n|\,H'|i\rangle}{(\omega_i-\omega_n)(\omega_i-\omega_m)}\right|^2 \\ &\times \delta(E_f - E_i - \hbar\omega), \end{aligned} \quad (4)$$

where E_i and E_f are the eigenvalues of initial and final states. $\hbar\omega$ is the photon energy absorbed by the initial state to reach to the final state. The delta function $\delta(E_f - E_i - \hbar\omega)$ is nonzero only if $E_f = E_i$ - $\hbar\omega$ is satisfied. The matrix element ,

$$\langle f|\,H'\,|i\rangle = -ie\sqrt{\frac{8\pi c^2}{\omega\hbar V}}\,\vec{\varepsilon}\cdot(E_i - E_f)\langle f|\,\vec{r}\,|i\rangle\,,$$

represents the electric dipole transition from an initial to the final states in terms of the $\vec{r}$-matrix element $\langle f|\vec{r}|i\rangle$ [21-23]. H' is the perturbed Hamiltonian due to the light-matter interaction. E, $\vec{\varepsilon}$, $\vec{r}$, ω, e, and t are the eigenvalues of matter, the polarization of radiation, the position vector, the angular frequency of radiation, the electronic charge of the electron, and the total time of transition, respectively. The RSA or positive nonlinearity is associated with the two-step excitation process through an intermediate state as described in Eq. (3) .

The excitation source of 532 nm (∼2.33 eV) is considered a resonant excitation source for the excitonic peaks at ∼627 nm (∼1.99 eV) and ∼520 nm (∼2.43 eV) while the non-resonant process occurs for excitonic peak at higher energies. It tells us that the one-photon excitation was located between A and B excitons, which are

assigned to the optical transition at the K/K' valley of the first Brillouin zone. The exciton binding energy [26, 27], the difference between electronic band gap and optical band gap, of a WS_2 monolayer is $\sim$0.71 eV at K valley [28]. The large binding energy is due to the significant reduction of dielectric screening on the Coulomb interactions in the 2D atomic layer semiconductor and the tightly bounded exciton with the strong Coulomb interaction [29]. Considering the large exciton binding energy of the WS_2 atomic layer, the A and B excitons of the WS_2 atomic layers could be excited to the deep conduction band by a two-step excitation through the optical band and by two-photon excitation through the virtual state or the broad optical band, respectively. Moreover, the C ($\sim$2.7 eV) and D ($\sim$3.54 eV) excitonic peaks could be excited to the optical band or conduction band with two-photon through a virtual state. It implies that the WS_2 atomic layer exhibited a larger ESA cross-section than the GSA cross-section for a given excitation source which is further confirmed by Fig. 3. It displays the nonlinear transmittance as a function of sample position for a given ratio of ESA to GSA cross-section using Eqs. (2) and (3).

The color map of Fig. 3 estimated the negligible nonlinear transmittance if ESA is equal to the GSA in their magnitudes. If the ratio of ESA to GSA is larger than 1, the nonlinear transmittance results in the RSA characteristics whereas the SA features are seen for a ratio less than 1. It revealed that the WS_2 atomic layer has a larger magnitude of ESA than GSA, which demands the involvement of C and D excitons in the optical transition process for given excitation energy as well.

Accuracy in Z-scan measurements

The third-order optical nonlinearity has been investigated by a set of techniques such as Z-scan, four-wave mixing, and spatial self-phase modulation etc. in the past decade [5, 30]. These techniques are designed to characterize the different parameters associated with cubic nonlinearity because of their own limitations and advantages for different optical materials. Among them, M. Sheik-Bahae et al developed the Z-scan technique, derived from the Gaussian beam profile, to investigate the real and imaginary part of third-order susceptibility [9, 31]. It is anticipated that the failure of the required experimental setup may mislead the research finding including the polarity of the NLA. Therefore, the Z-scan experimental setup is crucial for measurement accuracy. To obtain more accurate and reproducible results, the following factors are recommended to consider while designing the Z-scan experiment [15, 32].

a) System's nonlinearity: A variety of electronic and optical instruments are integrated into the Z-scan data acquisition process. Each of them has a unique polarization response to the electric field that might mislead the accuracy of the measurement. Therefore, selecting the system's linearity range for a given laser power (or intensity) is a key step to minimize the measurement uncertainty. Fig. 4 shows the schematic graph of the transmittance beam as a function of laser peak intensity without an optical sample to display the system's linearity ranges. It includes three different regions, namely, low intensity, moderate intensity, and high intensity, which we refer to the below 5 W/cm^2, in between 5 to 20 W/cm^2, and above 20 W/cm^2. The low-intensity region may not be enough excitation power for optical nonlinearity, the moderate intensity region shows linearity at which the experiment is suggested to conduct, and the higher intensity region is mostly saturated. In higher intensity region, the saturation limit of the detector would affect the measurement as well.

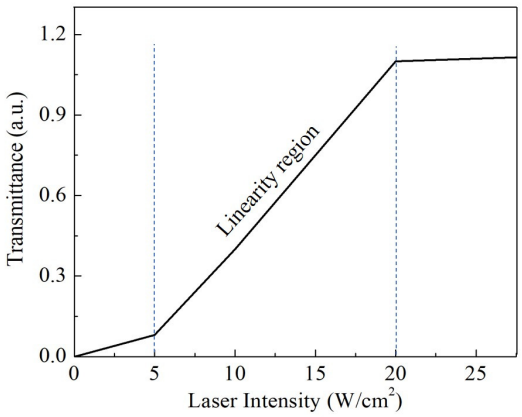

FIGURE 4. schematic graph of transmittance beam as a function of input intensity showing the linear and saturation region.

b) Optical nonlinearity from non-sample : The optical sample like nanoparticles, quantum dots, and two-dimensional materials are fabricated either on a suitable solid substrate or in the liquid base solution. Because of the narrow pulse and high laser power density, the transmittance measurement could include the additional polarization response to the electric field by the non-sample. It is recommended that the Z-scan experiment for only non-sample should be conducted under the same experimental condition before any measurement and then set the transmittance measurements results apart from the non-sample generated part in the experimental results [33].

c) Sample quality: In the Z-scan method, the beam is focused down along the z-axis which results in the variable laser power density along the laser direction. It indicates that the sample has interacted with the various laser intensity while moving along the z-axis. Inconsistency of

sample population or uneven doping in the optical sample may mislead the measurement accuracy. Therefore, it is recommended to use a high-quality sample uniformly distributed in the entire solid substrate or base solution. In specific, the concentration of the solution and the thickness of the sample pool should be uniform for the liquid-based sample. However, the sample growing method is very challenging and out of our control in some circumstances. So, the intensity scan (I-scan) technique is used to confirm the polarity of Z-scan data [34, 35].

d) Laser pointing accuracy and stability: The third-order optical nonlinearity is designed to collect the low-signal fluctuation transmittance by the detector. Therefore, it is sensitive to the power stability and its result on the measurement credibility. Stability depends on the laser quality itself, cavity instability, the current supplied, thermal effect, and many more. Therefore, two beams are designed in the Z-scan. The first beam is the reference beam that goes into the detector directly and the second beam interacts with the sample through the focusing lens before the detector. During the data analysis, the reference beam is used to normalize the nonlinear transmittance if the laser energy fluctuation is not big.

e) Thermal effect on the nonlinearity: The Z-scan technique, in general, is reliable for both pulse and CW laser sources. Also, the various laser specifications produce additional thermal mediated nonlinearity in the nonlinear transition process. It is reported that the thermal effect reorients the molecule of an optical sample or spatial alignment of atomic layers which affects the magnitude of a real coefficient of cubic susceptibility [30, 36]. To exclude the thermally induced optical nonlinearity, the repetition rate of the laser beam could be modified with a suitable chopper frequency during the measurements. But for pulse laser setup, selecting the materials having a shorter thermal diffusion time than pulse width is suitable as well.

f) Beam profile: The beam distribution in the Z-scan technique directly affects the measurements because the detector collects the spatial phase distortion of light-matter interaction. Therefore, the beam with a high-quality Gaussian beam with a single mode TEM_{00} beam is required for the pre-existing theoretical model. The Gaussian beam can be produced via a simple two-pin hole method [5].

g) Resolution and speed of moving sample: An adjustment of the sample moving resolution should be as small as possible. It implies that if position resolution is not small enough, we may lose the important transmittance information, especially in the valley or peak (z = 0) position. In addition, the speed of the optical sample should be uniform on the z-axis for keeping an equal interaction time between a sample and beam at each position. Therefore, the sample moving distance should be well-defined, and should not it be too big.

CONCLUSION

The polarity of NLA of the WS_2 atomic layer has been studied analytically. It demonstrates the RSA characteristics for a given excitation source as it has the larger ESA than GSA cross section. The excitation source of energy $\sim$2.33 eV is considered as a source for one photon excitation, which is located between A and B exciton absorption peaks. The optical transition associated with the WS_2 atomic layer is the two-photon transition which simply requires the existence of C and D excitonic peaks during the nonlinear transition process. The polarity of the NLA coefficient, in terms of the magnitude of ESA and GSA, demonstrated the physical origin of crossing from RSA to SA and vice versa. In addition, the factors that might affect the results from the Z-scan method have been discussed especially for experimentalists to improve the measurement accuracy and credibility. The WS_2 atomic layer with RSA phenomena has extensive technical applications in the areas of optical power limiting [37].

ACKNOWLEDGMENTS

This work is supported by the College of Arts and Sciences through funding number 101012 and Chemistry and Physics Department at The University of North Carolina at Pembroke.

EDITORS' NOTE

This manuscript was submitted to the Association of Nepali Physicists in America (ANPA) Conference 2022 for publication in the special issue of Journal of Nepal Physical Society.

REFERENCES

1. X. Zheng, Y. Zhang, R. Chen, Z. Xu, T. Jiang, *et al.*, "Z-scan measurement of the nonlinear refractive index of monolayer WS_2," Opt. express **23**, 15616–15623 (2015).
2. S. Yu, Q. Rice, T. Neupane, B. Tabibi, Q. Li, and F. J. Seo, "Piezoelectricity enhancement and bandstructure modification of atomic defect-mediated MoS_2 monolayer," Phys. Chem. Chem. Phys. **19**, 24271–24275 (2017).
3. E. A. R. González, A. Borne, B. Boulanger, J. A. Levenson, and K. Bencheikh, "Continuous-Variable Triple-Photon States Quantum Entanglement," Phys. Rev. Lett. **120**, 043601 (2018).
4. K. Zhang, M. Feng, Y. Ren, F. Liu, X. Chen, J. Yang, X.-Q. Yan, F. Song, and J. Tian, "Q-switched and mode-locked Er-doped fiber laser using $PtSe_2$ as a saturable absorber," Photon. Res. **6**, 893–899 (2018).
5. T. Neupane, S. Yu, Q. Rice, B. Tabibi, and F. J. Seo, "Third-order optical nonlinearity of tungsten disulfide atomic layer with resonant excitation," Opt. Materials **96**, 109271 (2019).

6. G.-B. Liu, W.-Y. Shan, Y. Yao, W. Yao, and D. Xiao, "Three-band tight-binding model for monolayers of group-VIB transition metal dichalcogenides," Phys. Rev. B **88**, 085433 (2013).
7. R. I. Woodward, E. J. R. Kelleher, R. C. T. Howe, G. Hu, F. Torrisi, T. Hasan, S. V. Popov, and J. R. Taylor, "Tunable Q-switched fiber laser based on saturable edge-state absorption in few-layer molybdenum disulfide (MoS_2)," Opt. Express **22**, 31113–31122 (2014).
8. J. Wang, B. Gu, H.-T. Wang, and X.-W. Ni, "Z-scan analytical theory for material with saturable absorption and two-photon absorption," Opt. Commun. **283**, 3525–3528 (2010).
9. M. Sheik-Bahae, A. A. Said, T. H. Wei, D. J. Hagan, and E. W. van Stryland, "Sensitive measurement of optical nonlinearities using a single beam," IEEE J. Quantum Electron. **26**, 760–769 (1990).
10. J. You, S. Bongu, Q. Bao, and N. Panoiu, "Nonlinear optical properties and applications of 2d materials: theoretical and experimental aspects," Nanophotonics **8**, 63–97 (2019).
11. D. W. Latzke, W. Zhang, A. Suslu, T.-R. Chang, H. Lin, H.-T. Jeng, S. Tongay, J. Wu, A. Bansil, and A. Lanzara, "Electronic structure, spin-orbit coupling, and interlayer interaction in bulk MoS_2 and WS_2," Phys. Rev. B **91**, 235202 (2015).
12. Y. Li, N. Dong, S. Zhang, X. Zhang, Y. Feng, K. Wang, L. Zhang, and J. Wang, "Giant two-photon absorption in monolayer MoS_2," Laser & Photonics Reviews **9**, 427–434 (2015).
13. S. Zhang, N. Dong, N. McEvoy, M. O'Brien, S. Winters, N. C. Berner, C. Yim, Y. Li, X. Zhang, Z. Chen, L. Zhang, G. S. Duesberg, and J. Wang, "Direct Observation of Degenerate Two-Photon Absorption and Its Saturation in WS_2 and MoS_2 Monolayer and Few-Layer Films," ACS Nano **9**, 7142–7150 (2015).
14. H. Zhang, S. B. Lu, J. Zheng, J. Du, S. C. Wen, D. Y. Tang, and K. P. Loh, "Molybdenum disulfide (MoS_2) as a broadband saturable absorber for ultra-fast photonics," Opt. Express **22**, 7249–7260 (2014).
15. T. Neupane, *Third-Order Optical Nonlinearity of Tungsten and Molybdenum Disulfide Atomic Layers*, Ph.D. thesis, Hampton, VA, USA (2020).
16. J. N. Coleman, M. Lotya, A. O'Neill, S. D. Bergin, P. J. King, U. Khan, K. Young, A. Gaucher, S. De, R. J. Smith, *et al.*, "Two-dimensional nanosheets produced by liquid exfoliation of layered materials," Science **331**, 568–571 (2011).
17. Z. Y. Zhu, Y. C. Cheng, and U. Schwingenschlögl, "Giant spin-orbit-induced spin splitting in two-dimensional transition-metal dichalcogenide semiconductors," Phys. Rev. B **84**, 153402 (2011).
18. T. Neupane, Q. Rice, S. Jung, B. Tabibi, and F. J. Seo, "Cubic Nonlinearity of Molybdenum Disulfide Nanoflakes," J. Nanosci. Nanotechnol. **20**, 4373–4375 (2020).
19. D. Kozawa, R. Kumar, A. Carvalho, K. Kumar Amara, W. Zhao, S. Wang, M. Toh, R. M. Ribeiro, A. H. Castro Neto, K. Matsuda, *et al.*, "Photocarrier relaxation pathway in two-dimensional semiconducting transition metal dichalcogenides," Nat. Commun **5**, 1–7 (2014).
20. A. Carvalho, R. Ribeiro, and A. C. Neto, "Band nesting and the optical response of two-dimensional semiconducting transition metal dichalcogenides," Phys. Rev. B **88**, 115205 (2013).
21. N. N. Srinivas, S. V. Rao, and D. N. Rao, "Saturable and reverse saturable absorption of Rhodamine B in methanol and water," J. Optical Society of America B **20**, 2470–2479 (2003).
22. N. Zettili, *Quantum Mechanics: Concepts and Applications* (Wiley, 2009).
23. C. M. Adhikari, *Long-Range Interatomic Interactions: Oscillatory Tails and Hyperfine Perturbations*, Ph.D. thesis, Rolla, MO, USA (2017).
24. C. M. Adhikari, V. Debierre, A. Matveev, N. Kolachevsky, and U. D. Jentschura, "Long-range interactions of hydrogen atoms in excited states. I. $2S-1S$ interactions and Dirac-δ perturbations," Phys. Rev. A **95**, 022703 (2017).
25. C. M. Adhikari, V. Debierre, and U. D. Jentschura, "Long-range interactions of hydrogen atoms in excited states. III. $nS-1S$ interactions for $n \geq 3$," Phys. Rev. A **96**, 032702 (2017).
26. M. M. Ugeda, A. J. Bradley, S.-F. Shi, F. H. Da Jornada, Y. Zhang, D. Y. Qiu, W. Ruan, S.-K. Mo, Z. Hussain, Z.-X. Shen, *et al.*, "Giant bandgap renormalization and excitonic effects in a monolayer transition metal dichalcogenide semiconductor," Nat. Mater **13**, 1091–1095 (2014).
27. A. Chernikov, T. C. Berkelbach, H. M. Hill, A. Rigosi, Y. Li, O. B. Aslan, D. R. Reichman, M. S. Hybertsen, and T. F. Heinz, "Exciton binding energy and nonhydrogenic Rydberg series in monolayer WS_2," Phys. Rev. Lett. **113**, 076802 (2014).
28. B. Zhu, X. Chen, and X. Cui, "Exciton binding energy of monolayer WS_2," Sci. Rep. **5**, 1–5 (2015).
29. K. He, N. Kumar, L. Zhao, Z. Wang, K. F. Mak, H. Zhao, and J. Shan, "Tightly bound excitons in monolayer WSe_2," Phys. Rev. Lett. **113**, 026803 (2014).
30. T. Neupane, H. Wang, W. Y. William, B. Tabibi, and F. J. Seo, "Second-order hyperpolarizability and all-optical-switching of intensity-modulated spatial self-phase modulation in $CsPbBr_{1.5}I_{1.5}$ perovskite quantum dot," Optics & Laser Technology **140**, 107090 (2021).
31. M. Sheik-Bahae, A. A. Said, and E. W. Van Stryland, "High-sensitivity, single-beam n_2 measurements," Optics letters **14**, 955–957 (1989).
32. J. Zhang, "Research on experimental accuracy of laser Z-scan technology," in *AIP Conference Proceedings*, Vol. 1794 (2017) p. 020025.
33. H. Zhang, S. Lu, J.-l. Zheng, J. Du, S. Wen, D. Tang, and K. Loh, "Molybdenum disulfide (MoS_2) as a broadband saturable absorber for ultra-fast photonics," Opt. express **22**, 7249–7260 (2014).
34. J. Seo, Q. Yang, S. Creekmore, and D. Temple, "Large pure refractive nonlinearity of nanostructure silica aerogel at near infrared wavelength," in *Proceedings of the 2nd IEEE Conference on Nanotechnology* (2002) pp. 495–497.
35. B. Gu, D. Liu, J.-L. Wu, J. He, and Y. Cui, "Z-scan characterization of optical nonlinearities of an imperfect sample profits from radially polarized beams," Appl. Phys. B **117**, 1141–1147 (2014).
36. T. Neupane, B. Tabibi, and F. J. Seo, "Spatial self-phase modulation in WS_2 and MoS_2 atomic layers," Opt. Mater. Express **10**, 831–842 (2020).
37. N. Dong, Y. Li, Y. Feng, S. Zhang, X. Zhang, C. Chang, J. Fan, L. Zhang, and J. Wang, "Optical limiting and theoretical modelling of layered transition metal dichalcogenide nanosheets," Sci. Rep. **5**, 1–10 (2015).